NANOSYSTEMS: PHYSICS, CHEMISTRY, MATHEMATICS, 2018, 9 (5), P. 631–640

$BiFeO_3$-Montmorillonite intercalated nano composites – synthesis and its characterization

K. Karthikeyan[1], A. Thirumoorthi[2,*]

[1]Research and Development centre, Bharathiar University, Coimbatore, Tamilnadu, India
[2]Assistant Professor, P. G. Department of Chemistry, Government Arts College, Udumalpet – 642 126, Tamilnadu, India

*dramoorthiudt@gmail.com

DOI 10.17586/2220-8054-2018-9-5-631-640

Bismuth Ferrite (BFO) intercalated Montmorillonite clay (MMT) nano composites have been synthesized using ascorbic acid and its optical behavior has been investigated. The characterization of BFO-MMT nano composites has been done using FT-IR, UV-visible, X-ray diffraction (XRD), Scanning Electron Microscope (SEM). Also, electron hole recombination has been investigated by photoluminescence (PL). From the analytical techniques, it has been found BFO entered into the layered host which was proved by elongation of basal plane and therefore agglomerated BFO was formed. The particle size can be calculated by Scherrer formula, is in good agreement with SEM. The strong absorption band in UV-Visible region attributed BFO nano composites can be used for photo catalytic degradation of Rhodamine-B (Rh-B). From the electrochemical studies, BFO-MMT clay nano composites showed a good specific capacitance at a scan rate of 10 mVs^{-1}.

Keywords: Bismuth ferrite, intercalation, montmorillonite clay, photoluminescence, specific capacitance.

Received: 19 February 2018

Revised: 20 September 2018

1. Introduction

The intercalation of new species into layered materials has great attraction in a wide range of applications [1]. The organic and inorganic guest species can easily be penetrated into the interlayer spaces of smectites to give intercalation compounds [2]. Zhaohui Han et al. [3] investigated the light absorbance and varying pore volume and pore size of CdS intercalated Laponite, Saponite, Hectorite, Montmorillonite clay (MMT). Peng Yuan et al. reported that synthesis of Fe-pillared interlayer clay samples possess good thermal stability and higher specific area with porosity [4]. The immobilization of MnS and NiS in the interlayer spaces of Montmorillonite and low luminescence intensities of MnS and NiS in Montmorillonite has been investigated by Nithima Khaorapapong et al. [5]. Also, Yasushige Mori et al. [6] have been reported that PL intensity was enhanced due to increase of particle surface area in Zinc sulphide nanoparticles suspended in Laponite XLG. The different photodecomposition behaviors of Rhodamine B on Laponite XLG and Montmorillonite have been studied by Peng Wang et al. [7].

The enhanced textural properties have been developed in two types of clay mineral/TiO_2 composites by Bahranowski et al. [8]. The enhanced textural properties of clay mineral was compared with TiO_2 and it was found that pillared montmorillonite materials have structural organization upon composite formation. They also found that the use of dialyzed clay mineral enhances strongly the adsorption properties of montmorillonite/TiO_2 composites obtained by conventional pillaring. Particularly, the specific capacitance behavior improved for nitrogen doped porous carbon ensemble on MMT nanocomposites of 223 Fg^{-1} at current density of 1 Ag^{-1} [9]. Montmorillonite has tetrahedral and octahedral sheet arrangement with gallery space and is shown in Fig. 1.

Bismuth ferrite (BFO) have been attracted considerable interest due to their unique optical and electrical properties, and a wide variety of potential applications for photovoltaic ferroelectric, piezoelectric, or magneto electric capabilities, as well as in spintronics [10–12]. $BiFeO_3$ constitutes a most important material being a semiconductor with the absorption edge in the visible region, $BiFeO_3$ NPs have been successfully tested in the degradation of Rhodamine B, methyl orange, methylene blue and bisphenol-A [13–15] and its capacitance properties have been improved by metal oxide doping [16].

From the literature survey, BFO can be used for optical, magnetic, photo catalytic applications and its capacitance behavior could be improved by doping with metal oxides. Additionally, capacitance properties has been enhanced by using layered types of materials such as Montmorillonite clay, layered doubled hydroxides (LDHs) in the form of composites. These facts spur us to synthesis the BFO intercalated MMT nanocomposites and investigate their capacitance and photocatalytic behaviors (Fig. 2).

In the present study, we report the synthesis of BFO and its intercalation into MMT clay to obtain nanocomposites of layered host of clay materials. The obtained composite was characterized using FT-IR, UV-Visible

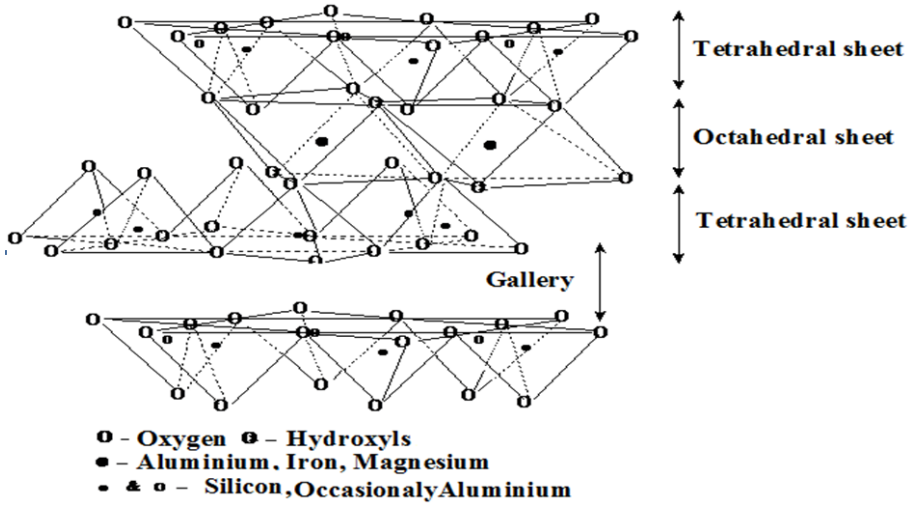

FIG. 1. Montmorillonite clay layered structure

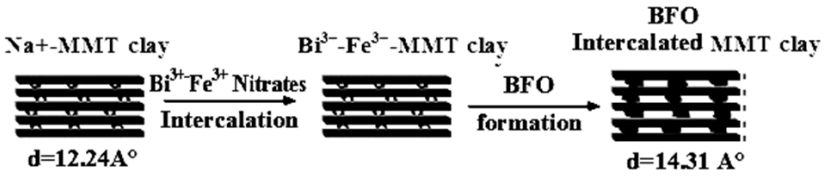

FIG. 2. A schematic diagram of BFO intercalated Na^{+}-Montmorillonite clay

spectra, XRD and SEM analysis, PL techniques. Also, the electrochemical behavior of BFO intercalated MMT nanocomposites for capacitance was investigated using Cyclic Voltammetric (CV) studies and the photo catalytic degradation of Rhodamine-B using intercalated BFO-Montmorillonite nanocomposites have been investigated.

2. Experimental section

2.1. Materials and methods

Bismuth nitrate [$Bi(NO_3)_3 \cdot 5H_2O$], Iron nitrate [$Fe(NO_3)_3 \cdot 9H_2O$], Ascorbic acid from Merck have been used as such without any further purification. Nitric acid and acetic acid from Merck of Analar grade reagents (A.R) were used as such and de-ionized water was used for the sample preparation.

2.2. Preparation of intercalated BFO

Bismuth nitrate and Ferric nitrate (in 1:1 molar ratio) were mixed with ascorbic acid and then add 1.2 mL of nitric acid (99.5 %). The solution was magnetically stirred at room temperature for 30 min. and the dark green colored solution was obtained. The mixture was vigorously heated until a dark brown solution was formed, then, the solution was cooled.

5 mM Fe/g clay suspension was taken and the cold BFO solution was added dropwise with constant stirring for about 24 h. where the intercalation took place [17]. The clay particles were converted into intercalated clay composites and then separated as yellow color clay composites. Then it was heated at 500 °C in Muffle furnace for 1h. to produce a brown clay.

2.3. Characterization of materials

UV-Visible absorption spectrum of the compound was recorded by using UV-Visible spectrometer (UV-1800, Shimadzu, Japan). FT-IR spectrometer of the type IR Prestige-21, Shimadzu, used to record IR spectrum using KBr pellets. The crystalline structure of BFO-MMT clay intercalated nano materials was identified by X-ray diffraction instrument (XRD, Shimadzu labX-6000). Sample morphology and size were examined using Scanning electron microscope (SEM, Jeol JSM-6390). The photoluminescence emission spectra of the samples were recorded with fluorescence spectrophotometer (PL, Horiba Jobin Yvon Flurolog-3). The cyclic voltammetric experiments

were carried out with a computer-controlled electrochemical working system (CH1660C Electrochemical Analyzer) between the scan rate of 10 mVs^{-1} and 50 mVs^{-1}.

3. Results and discussion

3.1. FT-IR analysis

FT-IR spectroscopy of pure MMT, BFO nanoparticles and BFO intercalated nanocomposites are shown in Fig. 3. The FT-IR spectroscopy data confirms acid activation of the clay. According to IR spectroscopic data Maria N. Timofeeva [18] reported that changes in chemical compositions in treatment with clay and leaching of Al^{3+} ions in octahedral sheet by the action of HNO_3 at the concentration of 0.125 – 0.5 mol/dm^3. The OH-bending frequencies of water 1633 cm^{-1} shift to 1625 cm^{-1} and this shift may be related to the interaction of HNO_3 with Al–OH groups.

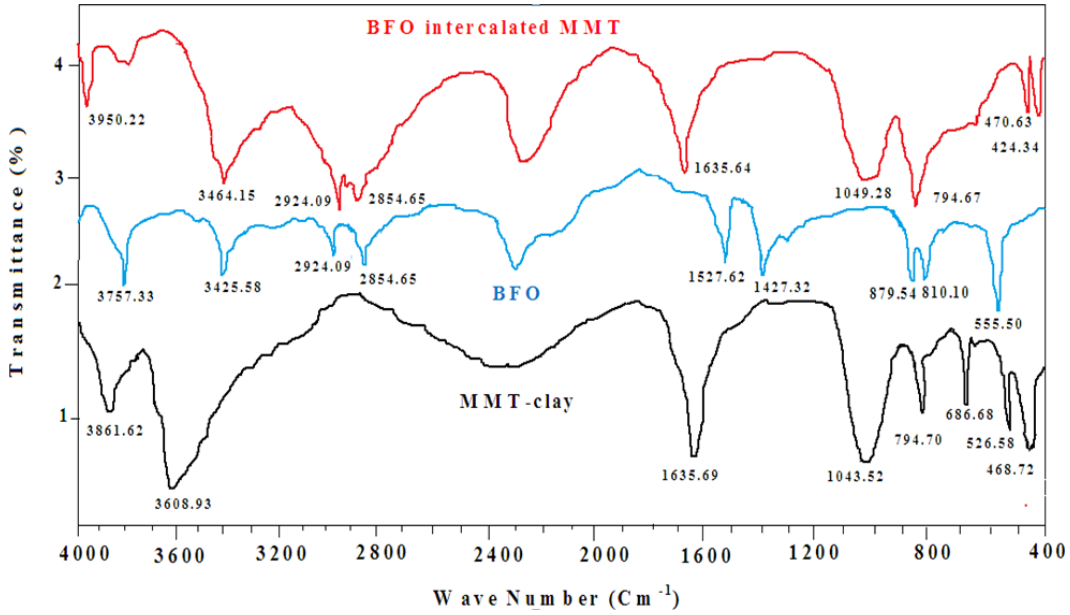

FIG. 3. FT-IR spectra of Pure Montmorillonite clay, BFO nano particles and BFO intercalated Composite

In our synthesized BFO intercalated MMT composites, the FT-IR spectral region discussed ranges from 400 – 4000 cm^{-1}. The comparison of wave number and assignment of peaks of pure MMT clay, BFO nano particles and intercalated BFO-MMT nanocomposites were listed in Table 1. The peak arises at 424.34 cm^{-1} for BFO intercalated MMT composites which confirm that BFO present in the MMT clay [19, 20]. The peak at 1635.69 cm^{-1} (due to O–H bending) does not shift and shows at 1635.64 cm^{-1} for BFO intercalated MMT due to absence of interaction of HNO_3 and Al–OH group of clay. The chemical composition (HNO_3 acid activation) changes in Montmorillonite clay and HNO_3 interaction with Al–OH group of clay was not takes place because of lower concentration of HNO_3 (0.04 mol/dm^3) for synthesis process. This has been confirmed using FT-IR spectra.

3.2. XRD analysis

X-ray diffraction patterns of Pure Na^+-Montmorillonite clay and BFO intercalated MMT clay nano composites are shown in Fig. 4(a) and (b) respectively. The XRD pattern of BFO shows pure rhombohedral perovskite structure, which are in good agreement with the powder data of JCPDS card number 86-1518 [21]. Montmorillonite clay not only shows their corresponding phase but also for quartz. The peaks 100, 101 and 110 planes corresponds to quartz and the peaks 001, 101 and 111 ($2\theta = 7.4$, 17.65 and 19.81 respectively) for MMT [22]. Manikandan et al. reported that the noble metal intercalated clay catalysts were very effective in selective hydrogenation reactions. They also found that Na-Montmorillonite clay shifted from $2\theta = 6.1°$ (d spacing value of 15 Å) to 1.5° (d spacing value of 59 Å). This confirms that the intercalation of BFO into clay minerals does not alter the crystal lattice structure, and hence, poor crystallinity of the nano composites [23]. Ecaterina Andronescu et al. reported that the diffraction peak of Montmorillonite clay (001 plane) shifts from $2\theta = 7.23°$ (basal spacing $d = 12.22$ Å) to 6.17° ($d = 14.31$ Å). The peak shifting to a lower diffraction angle is due to an increase in the clay basal spacing, which confirms the intercalation of nanoparticles in MMT interlayer spacing [24].

TABLE 1. Comparison of wave number of pure MMT clay and BFO-MMT nanocomposites

Montmorillonite clay		**BFO**		**BFO intercalated MMT nano composites**	
Peak position (cm^{-1})	Assignment	Peak position (cm^{-1})	Assignment	Peak position (cm^{-1})	Assignment
—	—	—	—	424.34	Fe–O stretching
468.72	Si–O–Si deformation	—	—	470.63	Si–O–Si deformation
526.58	Al–O–Si deformation	555.50	Fe–O stretching	—	—
686.68	Al–O and Si–O stretching	—	—	—	—
794.70	Si–O stretching	—	—	794.67	Si–O stretching
—	—	810.10 and 879.54	Fe–O and Bi–O frequencies	—	—
—	—	1427.32	C–H bending	—	—
—	—	1527.62	C=C stretching		
1043.52	Si–O–Si stretching	—	—	1049.28	Si–O–Si stretching
1635.69	OH-bending of water	—	—	1635.64	OH-bending of water
—	—	2854.65	C–H symmetric stretching	2854.65	C–H symmetric stretching
—	—	2924.09	C–H ssymmetric stretching	2924.09	C–H asymmetric stretching
3608.93	O–H stretching of water molecules	3425.58	O–H stretching of water molecules	3464.15	O–H stretching of water molecules
3861.62	O–H stretching of water molecules	3757.33	O–H stretching of water molecules	3950.22	O–H stretching of water molecules

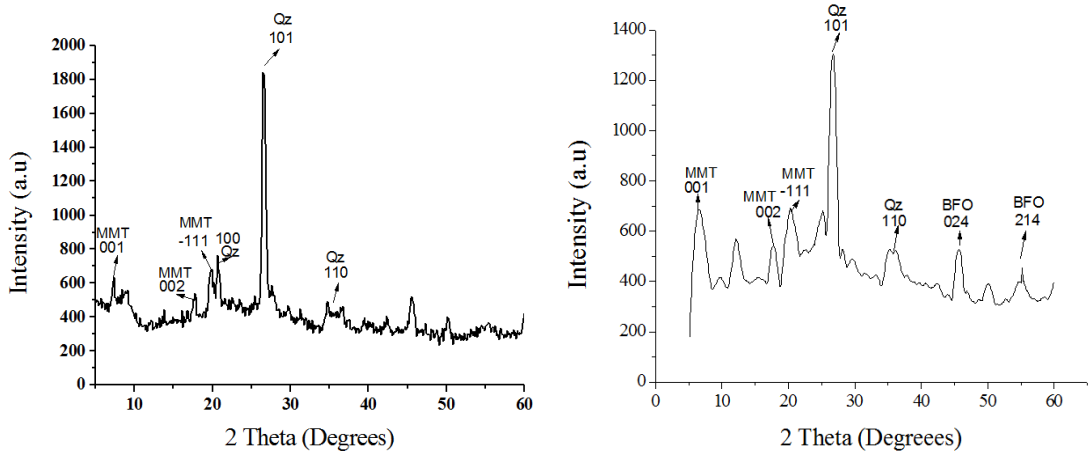

FIG. 4. XRD pattern of (a) Pure Montmorillonite Clay (b) BFO-MMT composites

From the literature survey, it has been observed that in BFO-MMT clay intercalation takes place, as a result the shifting of 2θ from 7.40° to 6.12°. In the present work, the XRD pattern of intercalated clay-bismuth ferrite was compared with untreated Montmorillonite clay and it has been found that untreated Montmorillonite clay (001 plane) peak at 2θ = 7.40° (basal spacing $d = 11.93$ Å), which corresponds to the spacing of clay layers, was shifted to 2θ = 6.12° (basal spacing $d = 14.41$ Å), due to intercalation of BFO in between the clay platelets. In MMT-BFO composites, the 024 and 214 planes were assigned to BFO phase (JCPDS card No. 86-1518) and the plane 024 for BFO was merged with MMT and hence the plane 214 at 55.3° was used to compute the size of BFO. Also, it has been observed that the increase in the basal spacing and the change in color of the products were caused by the intercalation of BFO and the formation of BFO in the interlayer spaces of MMT. The particle size of BFO can be estimated using the Debye Scherer formula:

$$2d = 0.9\lambda/\beta\cos\theta,$$

where β is the full width at half maximum intensity [FWHM] corresponding to then Diffraction angle 2θ in radian, and λ is the wave length of Cu-Kα radiation [25, 26]. The average crystallite size of the BFO nano particles was found to be 47.84 nm.

3.3. Scanning electron microscope

Figure 5(a) and (b) shows the SEM images of MMT-clay and BFO intercalated MMT-clay respectively. The preparation and sedimentation behavior of Montmorillonite clay-magnetite particles at various pH was reported by Galindo-Gonzalez et al. [27], suggesting that magnetic particles were well-adhered to sodium Montmorillonite clay in aqueous suspensions. The SEM images of magnetic covered clay particles at pH = 3 shows a great aggregation and at pH = 10 the coating was thinner leads to formation of less homogeneous particles. In SEM analysis, Vedhi et al. [28] found that a gradual change of uneven layered granular agglomerated clay – polymer nanocomposites to a fused well-organized layered morphology with flaky structure, predominantly due to clay mineral concentration. Figueras et al. [29] reported that the intercalation (d-space) decreases with enhancing the calcination temperature above 400 °C.

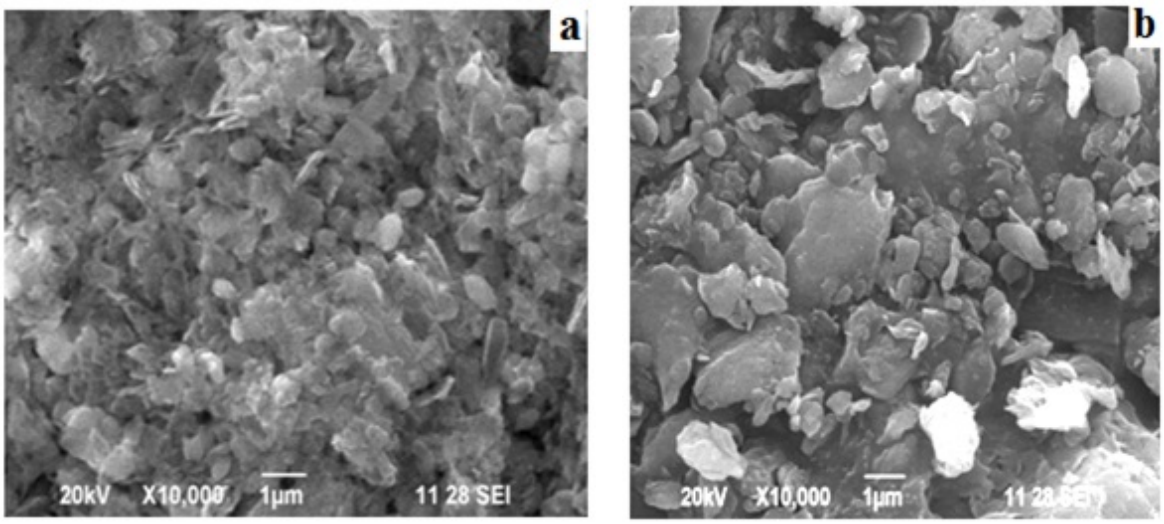

FIG. 5. SEM images of (a) MMT-clay (b) BFO intercalated MMT-clay

From the literature survey, it has been found that BFO-MMT nano composites only small amount of BFO intercalation takes place due to the calcination temperature at 500 °C. Also, the change of dense granular MMT clay morphology to uniform agglomerated flakes like shape of BFO due to intercalation and their crystallite size was found to be 47 nm shown in Fig. 4.

3.4. PL spectra

PL Spectra of pure MMT, BFO nano particles and BFO intercalated nano composite is shown in Fig. 6(a), (b) and (c) respectively. Dai et al. reported that $BiFeO_3$-Graphene nano composites have improved photocatalytic

activity of methyl orange and the peak was obtained at 429 nm [30]. Also Ramya et al. suggested that Montmorillonite clay peak has a maximum at 466 nm [31]. In the present studies, BFO nanoparticles and MMT shows acceptable peak range of 400 – 450 nm for BFO nano particle and 420 – 430 for MMT clay materials.

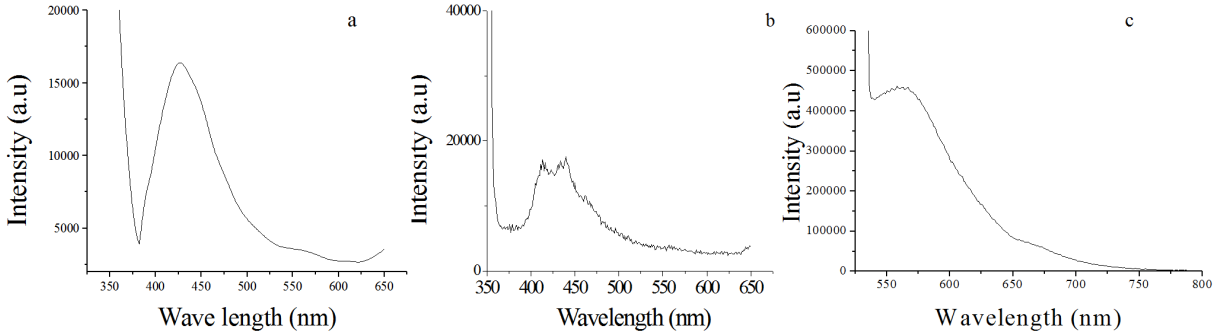

FIG. 6. Photoluminescence spectra of (a) Pure Montmorillonite (MMT) clay (b) Bismuth ferrite (BFO) and (c) BFO intercalated MMT nanocomposites

Yao et al. found that the optical behavior of $BiFeO_3$–KNSBN tri layer thin films and suggested that the multiple band gap energies are due to the combination of band gap energy of KNSBN and BFO films and the band centered at 530 – 540 nm due to the presence of oxygen vacancies [32]. The optical properties of BFO thin films have been studied at three different annealing temperatures. It has been found that the absorption shifts towards the longer wavelengths with increasing annealing temperature, suggesting that the band gap decreases with the annealing temperature. The optical band gap of the film was found to decrease from 2.67 eV to 2.57 eV with increasing temperature. Also two strong emissions around 2.53 and 2.36 eV were observed, indicating their potential applications as optoelectronic devices [33]. The PL spectrum of the pure BFO sample shows only one blue emission around 454 nm (2.73 eV) due to a self-activated center [34]. Sunil Chauhan et al. found that Mn-doped BFO samples gave two emission bands in the PL spectra [35]. The peak corresponding to 484 nm (2.56 eV) is due to blue emission band and dominant yellow-orange band is found at 570 nm (2.17 eV). The blue band emission around 484 nm in Mn doped BFO is due to a self-activated center and the shift of blue band to higher wavelength reported by Yu. X et al. owing to large crystallite size which leads to decrease in band gap. Based on this, they found the incorporation of Mn^{2+} in the BFO lattice [36]. From the literature [31] it has been found for nanocomposites of the type montmorillonite/chitosan/para pheylenediamine, the peak of MMT shifted towards higher wavelength region and red shift occurs.

It has been found that in BFO-MMT nanocomposites, the band shift occurs towards higher wavelength, thus producing a red shift. A band at around 570 nm (2.16 eV) for BFO-MMT composites confirms the intercalation (doping) of BFO in clay layered host. This emission will enhance the opportunities of intercalated BFO nano particles for both further fundamental studies and nano scale optical applications.

3.5. UV-Visible spectra

UV-Visible spectra of pure Montmorillonite clay, BFO, BFO intercalated MMT nanocomposites and their Tauc's plot are shown in Fig. 7(a,b,d) and (d) respectively. The absorption peaks of pure MMT and BFO corresponds to about 300 – 320 nm and 520 – 530 nm respectively and the band gap of BFO was found to be 1.75 eV.

In this present work, BFO intercalated MMT visible spectra shows a new peak at 256 nm and the band gap energy can be calculated by using Tauc's equation:

$$(\alpha h\nu)^n = k(h\nu - E_g),$$

where α is the absorption coefficient, k is the effective masses associated with the valence and conduction bands, n is 2 for a direct transition and 1/2 for an indirect transition, $h\nu$ is the absorption energy and E_g is the band-gap energy [37–39]. The band gap energy was found by extrapolating the linear portion of $(\alpha h\nu)^2$ against $h\nu$ plot to the point $\alpha = 0$ and is about 2.34eV [40]. The band gap changes from 1.75 eV to 2.34 eV and hence a prominent blue shift which may cause the reduction in particle size of BFO intercalated nanocomposites. The band gap of Ca and Ba doped BFO composites widened from 1.8 to 2.3 eV was attributed to dopant ions and hence reduction of particle size. The increase in band gap by doping significantly enhanced the photocatalytic efficiency of doped $BiFeO_3$ nanoparticles [41]. Thus, the band gap calculated for BFO-MMT nanocomposites coincides

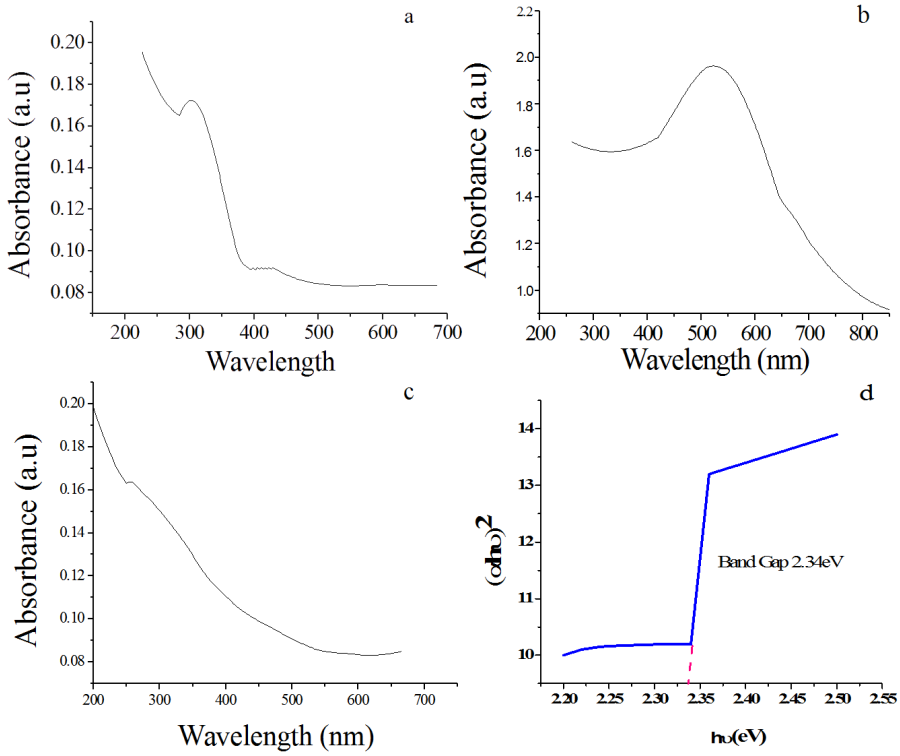

FIG. 7. UVVisible spectra of (a) Pure Montmorillonite (MMT) clay (b) Bismuth ferrite (BFO) and (c) BFO intercalated MMT nano composites (d) Taucs plot of BFO-MMT

with the literature available and hence BFO intercalated MMT may have a potential application as an appropriate photocatalyst for environmental remediation of organic contaminants under visible light irradiation.

3.6. Photocatalytic degradation

UV-Visible radiation is supported to photo catalytic degradation of BFO intercalated MMT. Rhodamine-B (RB) [0.05 g/L] was adsorbed onto Montmorillonite clay [0.05 g] at pH 7.0. Fig. 8 represents the UV-Visible spectra changes of RB in BFO-MMT clay suspension under visible irradiation. It was found that aqueous RB solution in the absence of BFO-Montmorillonite clay nano composites underwent no decomposition. Further, UV-Visible spectra changes as degradation of RB in the presence of BFO-MMT suspension under visible irradiation. The hypsochromic shift of absorption peak of RB gradually takes place from 556 to 524 nm after degradation. The hypsochromic shifts of the absorption peaks were found to result from the formation of N-deethylated mechanism [7].

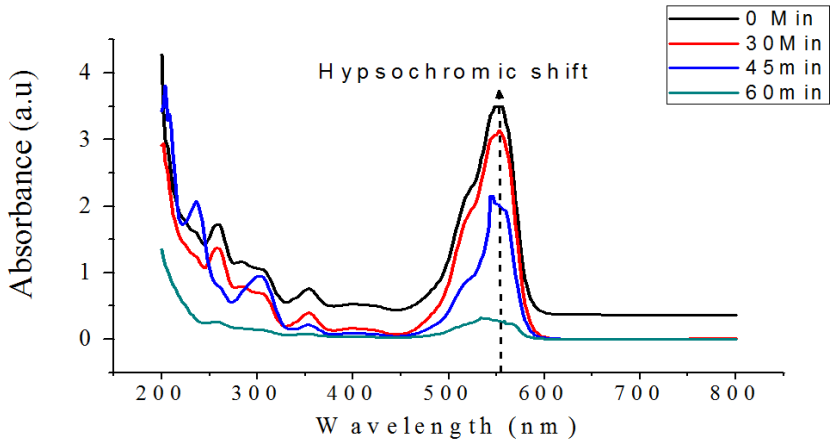

FIG. 8. Photo catalytic degradation of Rh-B by BFOMMT in various time intervals

3.7. Cyclic voltammetry

The electrochemical studies confirm the capacitance behavior of nano structured materials [42]. Baby Sunitha et.al [28] reported that o-toluidine polymerized with Montmorillonite by chemical oxidation method using potassium perdisulfate shows good solubility in both DMSO and DMF and the intercalation of the polymer in between the Montmorillonite clay layers increase in the d-spacing. Further, they found greater electrocatalytic response and stability, oxygen reduction ability and high conductivity using cyclic voltammetry and impedance studies. Ramesh et al. [43] reported that the incorporation of carbon nanotube and polyaniline with layered silicate of nano clay composites showed a higher capacitance of 331 Fg^{-1} at the scan rate of 10 mVs^{-1}. Hongjuan Li et al. [44] found from the electrochemical studies that MnO_2-pillared Ni^{2+}–Fe^{3+} layered double hydroxide nanocomposites exhibit large surface area and ideal capacitive behavior in neutral electrolyte and good cyclic properties.

The cyclic voltammograms of BFO-MMT nano composites have been investigated for their capacitance behavior in 1 mol L^{-1} NaOH at scan rate 10 – 50 mVs^{-1} with potential range -0.35 to 0.32 V is shown in Fig. 9. The CV studies gave anodic peak in positive and cathodic peak in negative potential directions. The specific capacitance of BFO-MMT nano composites at different scan rate of 10, 20, 30, 40 and 50 mVs^{-1} were 400, 262.5, 208, 169 and 155 Fg^{-1} respectively. At low scan rate of 10 mVs^{-1}, the material showed the good specific capacitance behavior due to porous layered structure and admirable electron accepting and donating behavior of montmorillonite clay. The decrease in capacitance with scan rates is attributed to the inner active sites that cannot completely proceed with the redox transitions at higher scan rates of CV and diffusion effect of proton within the electrode [45]. The decreasing trend of the capacitance suggests that the parts of the electrode surface are inaccessible at high charging-discharging rate. Hence, the specific capacitance obtained at the slowest scan rate reveals complete utilization of electrode material [46].

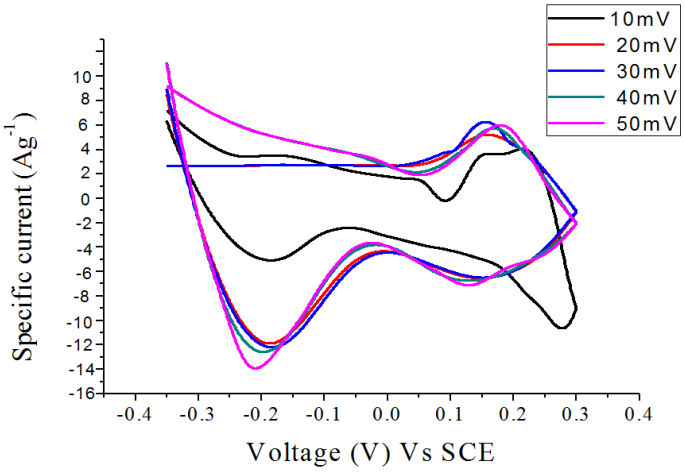

FIG. 9. Cyclic voltammetry of BFO-MMT at different scan rate

The effect of varying the scan rate with increasing peak current indicates the good adherence of the BFO-MMT composites on to electrode surface. The plot of logarithm of peak current against logarithm of scan rate is shown in Fig. 10, illustrates the current increases approximately in linear approach as described by the equation $y = 0.3936x + 0.195$; $R^2 = 0.9582$ for the anodic peak currents.

4. Conclusion

The BFO intercalated MMT nano composites were synthesized by intercalation using ascorbic acid as a supporter for improving capacitance behavior. The chemical composition changes of MMT clay affected by HNO_3 on clay, besides intercalation have been confirmed by FT-IR spectral studies. The intercalation of the BFO onto the clay layers, BFO crystalline size and composites, which are in nano scale, have been confirmed by XRD and SEM. The interaction between BFO and clay was confirmed by UV-Visible spectral analysis. The Tauc's plot showed the band gap of 2.34 eV supported for Photo catalytic activity Rhodamine-B dye in various time intervals. The photoluminescence peak revealed that luminescence behavior was improved and the band gap was found to be 2.16 eV. The electrochemical results confirmed the BFO-MMT nano composites had good specific capacitance of 400 Fg^{-1} in 1 mol L^{-1} NaOH solution at a scan rate 10 mVs^{-1}. Thus, the BFO-MMT nanocomposites can be used as a potential electrode material for capacitor applications.

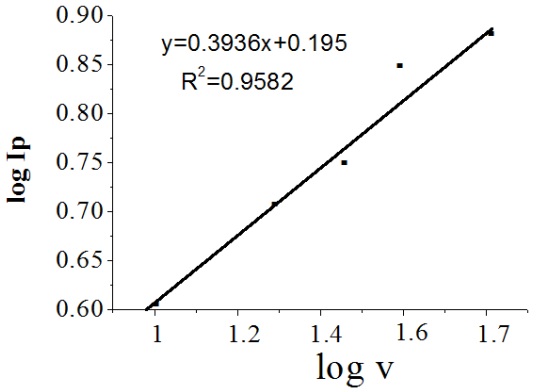

FIG. 10. Plot of anodic current against square root of scan rate

References

[1] Whittingham M.S., Jacobson A.J. *Intercalation Chemistry Academic Press*, New York, 1982, P. 1–18.

[2] Van Olphen H. *An Introduction to Clay Colloid Chemistry*, Wiley Inter science, New York, 1977.

[3] Zhaohui Hana, Huaiyong Zhu, et al. Nano composites of layered clays and Cadmium sulphide, Similarities and Difference in formation, Structure and properties. *Microporous and Mesoporous Materials*, 2008, **108**, P. 168–182.

[4] Peng Yuan, Faiza Annabi-Bergaya, et al. A combined Study by XRD, FTIR, TG and HRTEM on the Structure of delaminated Fe-intercalated/pillared clay. *Journal of Colloid and Interface Science*, 2008, **324**, P. 142–149.

[5] Nithima Khaorapapong, Areeporn Ontam, Jinda Khemprasit, Makoto Ogawa. Formation of MnS- and NiS- Montmorillonites by solid-solid reactions. *Applied Clay Science*, 2009, **43**, P. 238–242.

[6] Yasuyuki Arao, Yutaka Hirooka, Katsumi Tsuchiya, Yasushige Mori. Structure and Photoluminescence properties of Zinc Sulfide nanoparticles prepared in a Clay Suspension. *J. Phys. Chem. C*, 2009, **113**, P. 894–899.

[7] Peng Wang, Mingming Cheng, Zhonghai Zhang. On different photodecomposition Behaviours of Rhodamine B on Laponite and Montmorillonite Clay under visible light Irradiation. *Journal of Saudi Chemical Society*, 2014, **18**, P. 308–316.

[8] Bahranowski K., Gaweł A., et al. Influence of purification method of Na-Montmorillonite on textural properties of clay mineral Composites with TiO_2 Nano particles. *Applied Clay Science*, 2017, **140**, P. 75–80.

[9] Wengwen Zhang, Zhenbo Ren, et al. Activated Nitrogen-doped porous carbon ensemble on montmorillonite for high-performance supercapacitors. *Journal of alloy and compounds*, 2018, **743**, P. 44–52.

[10] Zang Y., Xie D., et al. Enhanced photovoltaic properties in grapheme/ polycrystallineBiFeO3/Pt hetero-junction structure. *Appl. Phys. Lett.*, 2011, **99**, P. 132904.

[11] Yang S.Y., Seidel J., et al. Above-band gap voltages from Ferroelectric photovoltaic devices. *Nat. Nanotechnol.*, 2010, **5**, P. 143–147.

[12] Nguyen Anh Tien, Chau Hong Diem, et al, Structural and Magnetic properties of $YFe_{1-x}Co_xO_3$ ($0.1 \leq x \leq 0.5$) perovskite nano materials synthesized by Co-precipitation method. *Nanosystems: Physics, Chemistry, Mathematics*, 2018, **9** (3), P. 424–429.

[13] Yang J., Li X., et al. Factors controlling pure-phase Magnetic $BiFeO_3$ powder synthesized by Solution combustion synthesis. *Alloys Compd.*, 2011, **509** (37), P. 9271–9277.

[14] Xian T., Yang H., et al. Photo catalytic properties of $BiFeO_3$ nano particles with different sizes. *J. Mater. Lett.*, 2011, **65**, P. 1573–1575.

[15] Gao F., Chen X., et al. Visible-Light Photocatalytic Properties of Weak Magnetic $BiFeO_3$ Nano particles. *J. Adv. Mater.*, 2007, **19**, P. 2889.

[16] Lokhande C.D., Dubal D.P. Oh-Shim joo. Metal Oxide thin film based supercapacitors. *Current applied Physics*, 2011, **11**, P. 255–270.

[17] Doff D.H., Gangas N.H.J., Allan J.E.M., Coey J.M.D. Preparation and Characterization of iron oxide pillared Montmorillonite. *Clay minerals*, 1988, **23**, P. 367–377.

[18] Timofeeva M.N., Panchenko V.N., et al. Effect of nitric acid modification of montmorillonite clay on synthesis of solketal from glycerol and acetone. *Catalyst Communications*, 2017, **90**, P. 65–69.

[19] Peng Yuan, Faiza Annabi-Bergaya, et al. A Combined study by XRD, FTIR, TG and HRTEM on the Structure of delaminated Fe-intercalated/pillared Clay. *Journal of colloid and Intreface Science*, 2008, **324**, P. 142.

[20] Yohannan Panicker C., Hema Tresa Varghese, Daizy Philip. FT-IR, FT-Raman and SERS spectra of Vitamin C. *Spectochimica Acta Part A*, 2006, **65**, P. 802–804.

[21] Tayyebe Soltani, Mohammad H. Entezari. Sono-synthesis of bismuth ferrite nanoparticles with high photocatalytic activity in degradation of Rhodamine B under solar light irradiation. *Chemical engineering Journal*, 2013, **223**, P. 145–154.

[22] Anna Rokicinska, Piotr Natkanski, et al. Co_3O_4-pillared montmorillonite catalyst synthesized by hydrogel-assisted route for total oxidation of toluene. *Applied catalyst B; Environmental*, 2016, **195**, P. 59.

[23] Manikandan D., Mangalaraja R.V., Ananthakumar S., Sivakumar T. Synthesis of metal intercalated clay catalysts for selective hydrogenation reactions. *Catalyst in Industry*, 2012, **4**, P. 215–230.

[24] Ruxandra Irina Iliescu, Ecaterina Andronescu, et al. Montmorillonite-alginate nanocomposite beads as drug carrier for oral administration of carboplatin – Preparation and characterization. *U. P. B. Sci. Bull., Series B*, 2011, **73**, P. 3.

[25] Min Zhang, Zhenfa Zi, et al. Size Effects on Magnetic Properties of $Ni_{0.5}Zn_{0.5}Fe_2O_4$ Prepared by Sol-Gel Method. *Advances in Materials Science and Engineering*, 2013, 609819, 10 pp.

[26] Ajin Sundar S., Joseph John N. Synthesis and studies on structural and optical properties of zinc oxide and manganese-doped zinc oxide Nanoparticles. *Nanosystems: Physics Chemistry Mathematics*, 2016, **7**, P. 1024–1030.

[27] Galindo-Gonzlez C., De Vicente J., et al. Preparation and Sedimentation Behavior in Magnetic Fields of Magnetite-Covered Clay Particles. *Langmuir*, 2005, **21**, P. 4410.
[28] Baby Suneetha R., Vedhi C. Synthesis, characterization and electrochemical behaviour of Montmorillonite Poly(o-toluidine) nano composites. *Applied Clay Science*, 2014, **88–89**, P. 18–25.
[29] Figueras F., Klapyta Z., et al. Use of competitive ion exchange for Intercalation Of montmorillonite with Hydroxy-aluminum cpecies. *Clay and clay Minerals*, 1990, **38**, P. 257–264.
[30] Dai J.F., Xian T., Di L.J., Yang H. Preparation of $BiFeO_3$-Graphene Nano composites and their Enhanced Photo Catalytic Activities. *Journal of Nano Materials*, 2013, 642897, 5 pp.
[31] Ramya E., Rajashree. Ch. Nayak., Narayana Rao P.L. New Hybrid organic polymer montmorillonite /chitosan/ Polyphenyenediamine composites for nonlinear optical studies. *Applied clay science*, 2017, **150**, P. 323-332.
[32] Yao Y.B., Mak C.L. Optical, ferroelectric and magnetic properties of Multi ferroelectric $BiFeO_3$–$(K_{0.5}Na_{0.5})_{0.4}(Sr_{0.6}Ba_{0.4})_{0.8}$ Nb_2O_6. *Thin films Journal of Alloys and Compounds*, 2014, **586**, P. 448.
[33] Bobby singh soram, Boinis singh ngangom, Sharma H.B. Effect of annealing temperature on the structural and optical properties of sol-gel processed nano crystalline $BiFeO_3$ thin films. *Thin solid film*, 2012, **524**, P. 57–61.
[34] Dillip K. Mishra, Xiaoding Qi. Energy levels and photoluminescence properties of Nickel-doped bismuth Ferrite. *Journal of Alloys and Compounds*, 2010, **504** , P. 27–31.
[35] Sunil chauhan, Manoj Kumar, et al. Multiferroic, Magnetoelectric and optical properties of Mn doped $BiFeO_3$ nano particles. *Solid state Communications*, 2012, **152**, P. 525–529.
[36] Yu X., An X., Enhanced Magnetic and optical properties of Pure and (Mn, Sr) doped $BiFeO_3$ nano crystals. *Solid state communications*, 2009, **149**, P. 711.
[37] Yoon M., Seo M., et al. Synthesis of Liposome-Templated Titania Nanodisks: Optical Properties and Photocatalytic Activities. *Chem. Mater.*, 2005, **17**, P. 6069–6079.
[38] Li L., Yang Y., et al. Fabrication and charecterization of single- Crytalline ZnTe Nano wire Arrays. *J. Phys. Chem. B*, 2005, **109**, P. 12394–12398.
[39] Arulmozhi S., Packiaseeli V., Rajendran R., Vijayalakshmi. Structural, Optical and morphological study of Tungsten selenide thin film. *Nanosystems: Physics, Chemistry, Mathematics*, 2016, **7**, P. 703–706.
[40] Huo Y.N., Jin Y., Zhang Y. Citric acid assisted solvothermal synthesis of $BiFeO_3$ Micro spheres with high VisibleLight photocatalytic activity. *J. Mol. Cat. A: Chem.*, 2010, **331**, P. 15–20.
[41] Bhusahan B., Das D., et al. Enhancing the magnetic characteristics of $BiFeO_3$ nano particles by Ca, Ba co-doping. *Material chemistry and physics*, 2012, **135**, P. 144–149.
[42] Balasubramaniam M., Balakumar S. Effect of precipitating agent NaOH on the Prpapration of copper oxide nanostructures for electrochemical applications. *Nanosystems: Physics, Chemistry, Mathematics*, 2016, **7**, P. 482–487.
[43] Ramesh Oraon, Amrita Adhikari, Santosh Tiwari, Ganesh Chandra Nayak. Enhanced specific capacitane of self- assembled three dimentional CNT/ Layered Silicate/ Polyaniline hybrid sandwiched nanocomposite for Supercapacitor application. *ACS Sustainable chemistry & Engineering*, 2016, **4** (3), P. 1392–1403.
[44] Hongjuan Li, Gang Zhu, et al. Preparation and Capacitance property of MnO_2-pillared Ni^{2+}-Fe^{3+} layered double hydroxide nanocomposite. *Journal of Colloid and Interfac Science*, 2010, **345**, P. 228–233.
[45] Kotz R., Carlen M. Principle and application of electrochemical capacitors. *Electrochem. Acta*, 2000, **45**, P. 2483.
[46] Lokhande C.D., Gujar T.P., Shinde V.R., Rajaram S. Mane. Electrochemical Super capacitor application of Perovskite thin films Sung-Hwan Han. *Electrochemistry communications*, 2007, **9**, P. 1805–1809.